Rotor Topology Optimization of Interior Permanent Magnet Synchronous Motor With High-Strength Silicon Steel Application

Lingyu Gao[1,2], Hang Zhang[2,3], Lubin Zeng[2], and Ruilin Pei[1]

[1]School of Electrical Engineering, Shenyang University of Technology, Shenyang 110870, China
[2]Inn-Mag New Energy Ltd., Suzhou 215000, China
[3]School of Mechanical Engineering, Université de Technologie de Troyes, 10004 Troyes, France

This article presents the rotor optimization in an interior permanent magnet synchronous machine (IPMSM) with high-strength non-grain-oriented (NGO) silicon steel material. Different from simple replacement with high-strength NGO, this article presents a customized design to make the best use of rotor iron core material. Specific optimization of the rotor topology is presented, followed with simulation verification by finite element method (FEM). Based on the simulation results, the benefits and limitations of the optimization design with the replacement of high-strength NGO are listed. In order to further overcome the limitations of the presented optimization design, magnetic characteristics of the high-strength NGO laminations subjected to various tensile stresses are measured in the experiment. Finally, experimental results are analyzed, and the conclusions to employ high-strength NGO for IPMSM are summarized.

Index Terms— **High-strength non-grain-oriented (NGO) silicon steel, interior permanent magnet synchronous machine (IPMSM), iron loss, rotor design.**

I. Introduction

In recent years, there is a trend of electrification with the consumption of non-renewable fossil fuel. Especially in the automotive application, the demand of new energy vehicles (NEVs) has been increasing year by year. The system of NEV can be divided into three major subsystems: battery system, control system, and electric drive system [1]. For the electric drive system, facilitating with interior permanent magnet synchronous machine (IPMSM), the power, output torque, and efficiency are strongly dependent on the steel lamination material properties. The requirements for the material properties can be summarized as follows. The iron loss in the steel should be low for the high efficiency under high-speed operation. Moreover, the saturated flux density in the core should be increased to ensure high output torque as well as overload capability. As for rotor core material, its mechanical properties determine the maximum operation speed [2].

The new material research for electric motor application is usually based on the conventional topology design and operating platform with the single replacement of material. In recent years, more advanced research has illustrated that replacing conventional materials can not only improve the performance of electric motors, but also affect the motor parameter design. Therefore, the electric motor, with customized design according to the material characteristics, can make the best use of the applied new materials. For example, Cicalé *et al.* [3] have investigated the electric motor structural design with grain-oriented (GO) silicon steel. Since the GO silicon steel only exhibits great electromagnetic characteristics in the rolling direction, the segmented stator structure was applied in [3]. Reddy *et al.* [4] investigated the rotor topology design of a switched reluctance motor (SRM) using a dual-phase material. The material was formed by magnetic ferrite phase and non-magnetic austenite phase, achieved by nitriding the rotor magnetic bridges and center-posts after lamination. Therefore, the topology of optimized rotor can adopt different designs considering the different material properties. In IPMSM rotor topology design, the magnetic bridge and center-post can also influence the output torque characteristic by reducing the leakage flux. Hence, Tietz *et al.* [5] conducted an IPMSM rotor topology design by narrowing magnetic bridge to reduce leakage flux. The thickness of rotor magnetic bridge and post are limited by yield strength of the rotor material. Therefore, materials with better mechanical properties can minimize the width of the magnetic bridge to gain better machine characteristics. To achieve this goal, high-strength non-oriented silicon steel is used in the optimization of IPMSM rotor structure in [6]. However, narrowing magnetic bridge and post will increase the magnetic saturation level of material, also, partial magnetic saturation zone and core loss concentration zone will be generated. The magnetic saturation zone is also the concentration zone of the tensile stress, which can actually deteriorate the core loss characteristic.

This article aims at proposing a systematic optimization design for IPMSM rotor utilizing high-strength non-GO (NGO) silicon steel with the consideration of both magnetic saturation and mechanical stress. The rotor optimization is coordinated with multiple project parameters for specific project examples.

This article is organized with four sections. In Section II, the rotor topology optimization by using high-strength NGO in high-speed IPMSM is presented, including rotor parametric

Manuscript received May 8, 2020; revised August 14, 2020 and September 24, 2020; accepted September 27, 2020. Date of publication September 30, 2020; date of current version January 20, 2021. Corresponding author: R. Pei (e-mail: peiruilin@inn-mag.com).

Color versions of one or more figures in this article are available at https://doi.org/10.1109/TMAG.2020.3027893.

Digital Object Identifier 10.1109/TMAG.2020.3027893

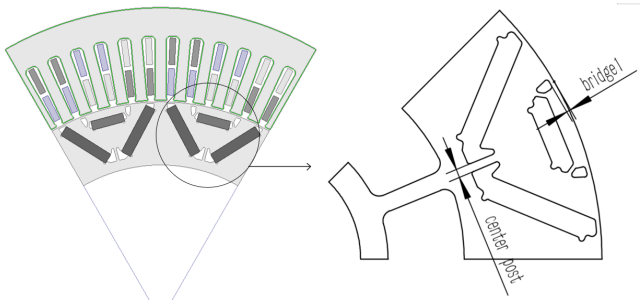

Fig. 1. IPMSM rotor parametric topology.

design specification and optimization results analysis by finite element method (FEM) simulation. Section III mainly introduces the experiment design with high-strength NGO subjected to various frequency and tensile stress. In Section IV, the general conclusion of IPMSM rotor design with high-strength NGO is summarized.

II. Rotor Topology Design and Simulation Result Analysis With High-Strength NGO Application

Compared with conventional NGO in IPMSM rotor design, the iron loss can be slightly higher when the high-strength NGO steel is employed. Nevertheless, the yield strength of this material has been significantly improved meanwhile. Gong [7] has introduced the specific methods to improve the yield strength. In Japan, the yield strength of high-strength NGO has already reached between 570 and 780 MPa at the end of the last century [7], [8]. In China, the investigation and production of these materials started lately. The applied material is SW35YS600 high-strength NGO in this article and the yield strength of the 0.35 mm thick material has raised to 600 MPa (theoretically) through solid solution strengthening method. Although the growth is limited, the yield strength has increased by 50% compared with 400 MPa of the traditional B35A270. The improvement in material yield stress can significantly affect the rotor parameter design. The presented IPMSM possesses a peak speed of 12 000 r/min, in which the rotor adopts a delta-shaped topology, as shown in Fig. 1. Section II-A in this part mainly presents the optimization of rotor topology and the improvement of IPMSM performance with high-strength NGO.

A. Rotor Topology Optimization

In rotor design, the magnetic bridge and center-post widths can be set as optimization parameters as shown in Fig. 1. In the rotor magnetic path, magnetic flux generated by PMs interacts with the stator flux to produce air-gap flux and then output torque. However, forming a closed loop inside the rotor, a small part of the rotor flux is consumed to be leakage flux. For the sake of reducing leakage flux ratio, the widths of bridges and post should be designed as small as possible. The maximum speed of the presented prototype can reach 12 000 r/min. With the safety factor of 1.2, the maximum design speed should reach 14 400 r/min. As a result, PMs will generate a large centrifugal force to compress the rotor iron core. The connected magnetic bridge part is usually

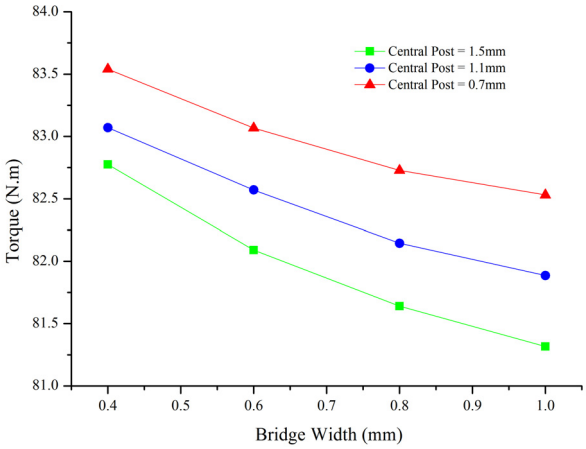

Fig. 2. Maximum output torque improvement of IPMSM.

in tensile stress concentration zone and is subjected to the maximum centrifugal force. The allowable stress equals to yield strength, for which the minimum widths of bridges and post are restricted by the yield strength of the rotor iron core material. The iron loss generated by the rotor accounts for a rather low ratio compared with the overall loss. As a result, the widths of bridges and posts should be considered carefully, to limit leakage flux and enhance the IPMSM performance by reducing the rotor iron loss increased with new material application.

B. Simulation Result Analysis by FEM

In this article, an IPMSM parametric 2-D model is applied to optimize the widths of bridges and center-post. When the centrifugal force satisfies the yield strength limit of high-strength NGO, the widths of bridges and post are minimized. The optimization results illustrate that the maximum output torque can be increased by 12 N·m (shown in Fig. 2) and the high-efficiency zone can be expanded (shown in Fig. 3), as the width of bridges is reduced from 1.0 to 0.4 mm, and that of center-post is varied from 1.5 to 0.7 mm.

According to the simulation results, the output capability is enhanced after optimization but shortcomings still exist. Due to high rotation speed, the electrical frequency in the magnetic field is relatively high. It is known that the iron loss includes hysteresis loss, eddy current loss, and abnormal loss. Under high-frequency operation, eddy current loss and abnormal loss will rise distinctly. According to the theoretical formula, the eddy current loss is proportional to the square of the excitation frequency and sustained magnetic field density. Due to the reduction of the widths, the leakage flux can be reduced, with the sacrifice of magnetic flux density concentration. Under the peak conditions, the magnetic density distribution sustained at the bridge part has increased from 2.10 to 2.32 T calculated by FEM simulation. The same increasement has been achieved with the iron loss distribution, the corresponding peak iron loss value has increased from 4.27E5 to 5.56E5 W/m^3, as shown in Fig. 4. At the same time, the widths of bridges and post are greatly reduced, and higher requirements are imposed on the manufacture of punching die, which leads to an increasement in the overall cost.

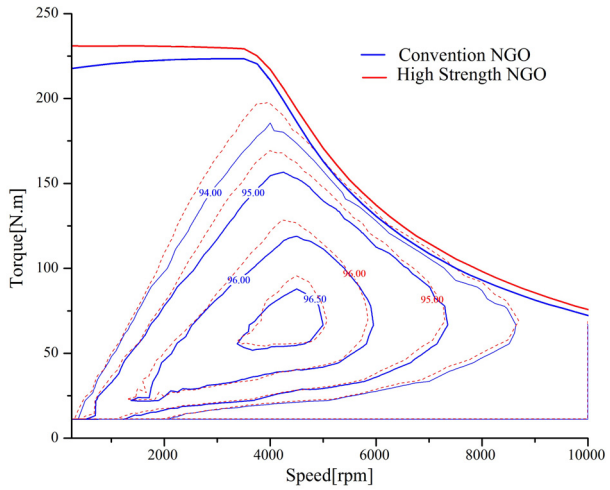

Fig. 3. Efficiency MAP with conventional and high-strength NGO.

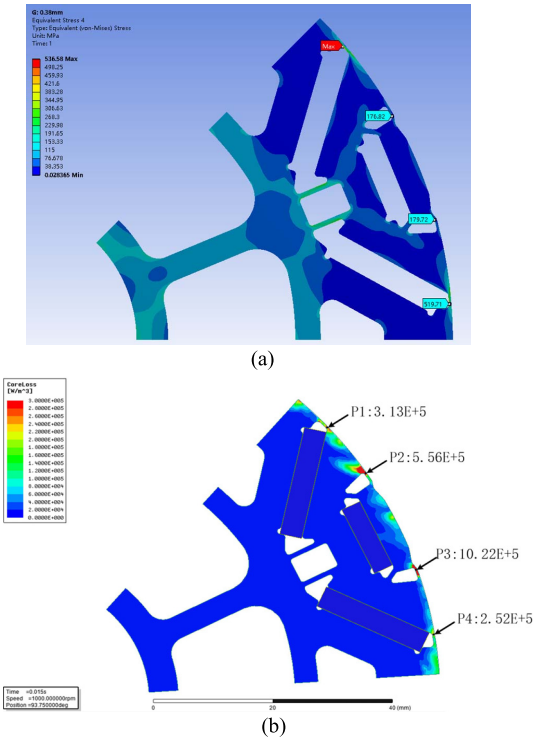

Fig. 4. Rotor topology design adopting narrow magnetic bridge and center post method. (a) Equivalent von-Mises stress distribution on rotor. (b) Core loss distribution on rotor.

III. Experiment Research of High-Strength NGO Magnetic Characteristic Under Tensile Stress

According to the above FEM calculation results, we can know that the introduction of high-strength NGO materials is beneficial to improve the centrifugal force withstanding capability of the rotor laminated core in the high-speed operation. Combined with the topology optimization of rotor magnetic bridges and center-posts, the electromagnetic performance can be improved for electric motor application. In Section II, the limitation of this design is also presented. Reducing the width of bridges and posts will increase the magnetic reluctance. Therefore, the flux density and loss distribution on the rotor will be concentrated with the decreasing of the bridge width. The magnetic flux density concentration can partially cause the material saturation at bridges and posts of the rotor. Thus, the magnetic permeability will be greatly reduced and the overall efficiency of the electric motor will be affected by the loss concentration part.

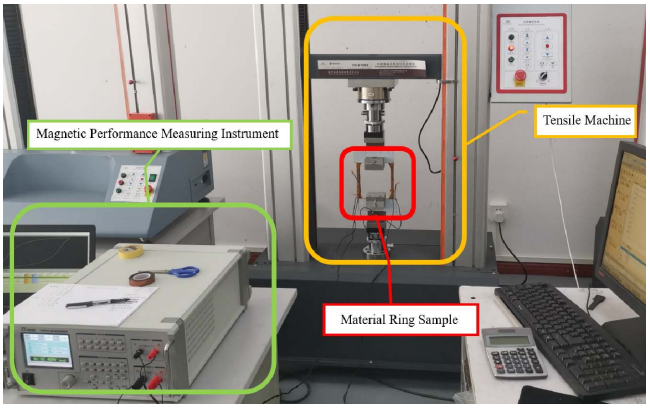

Fig. 5. Electromagnetic characteristics measurement under tensile stress.

However, under the actual operating condition, the position of the bridges and posts is also in a state where the tensile stress is concentrated from the rotating centrifugal force generated by the rotor PMs. When the NGO material is magnetized, it is easier to form 180° magnetic domains with higher permeability under tensile stress, so that the loss characteristics will actually be improved. In actual operating condition, the iron loss concentration can be actually improved or the saturation may not be appeared due to the concentration of tensile stress. Up to date, the material properties of the high-strength NGO under different stress application have not been reported in the previous literature. Based on this fact, the magnetic properties of the high-strength NGO (SW35YS600) have been measured under the conditions of variable excitation field, frequency, and tensile stress. Sections III-A and III-B will focus on the experiments set up and the results analysis. The design of this experiment intends to conduct a more in-depth study of the material properties with high-strength NGOs and its potential application in high-speed IPMSM.

A. Experiment Set-Up

Four subsets of experiments have been conducted in the overall experiments set-up: 1) standard tensile experiment; 2) tensile experiment of non-standard ring sample; 3) electromagnetic characteristic measurement by ring sample method; and 4) electromagnetic characteristic measurement by ring sample method with various tensile stress application. The experimental group is the high-strength NGO (SW35YS600), while the control group is the conventional NGO (B35A270). The experimental group and the control group are fabricated to the same size with the application of electrical wire cutting. Then ten pcs of the single sheet of experimental group and control group are cemented by adhesives. Both sides of the ring sample are wound with coils to measure the electromagnetic properties. Both sides with windings are subjected to varying tensile stresses. Experiments gear set-up is shown in Fig. 5.

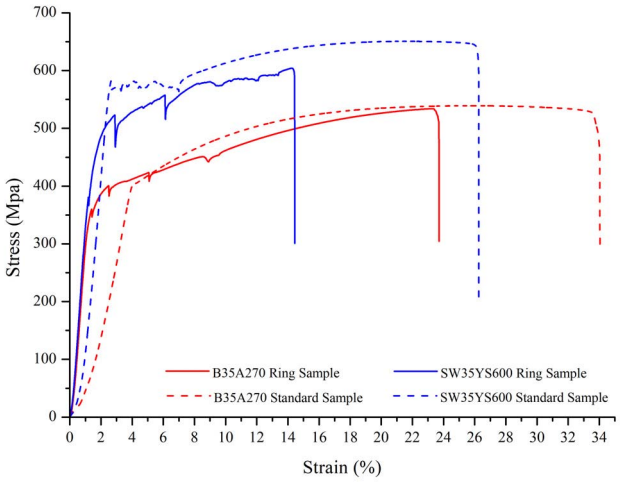

Fig. 6. Tensile experiment result comparison.

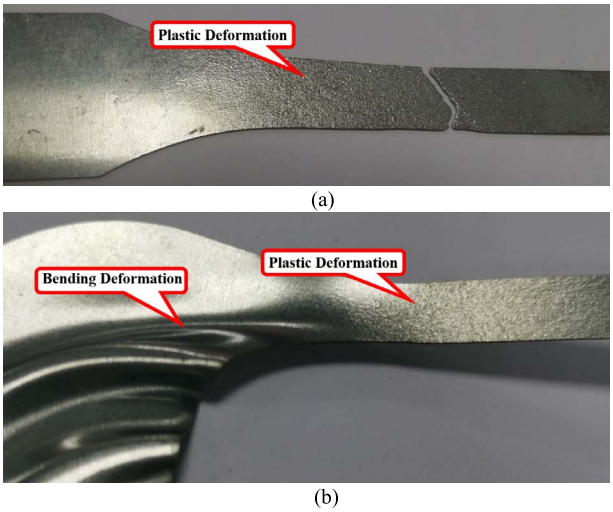

Fig. 7. Sample rupture comparison. (a) Sample rupture after standard tensile experiment. (b) Ring sample rupture after tensile experiment.

The principle of the experimental design is illustrated as follows. Firstly, the stress–strain curves obtained in experiment 1 are used as the standard. Comparing the results of experiments 1 and 2, we can observe that the interference of the ring sample topology can be eliminated by adjusting the stress–strain curves in experiment 2 to the standards. Then, the electromagnetic characteristic curves measured by the Epstein method are used to be the standard. Adjusting the curves obtained in experiment 3 to the standard electromagnetic curves can eliminate the interference of the ring sample topology and measurement. Finally, through the adjusted characteristic curves of experiments 2 and 3, the curves obtained in experimental 4 can be adjusted and compared.

B. Experiment Result Analysis

In the standard tensile experiment 1, the stress–strain curves with conventional NGO and high-strength NGO are compared in Fig. 6. In the experiment results, the yield strength of the conventional NGO achieves 402.70 MPa. Considering the safety factor of 1.2, the maximum allowable stress for the high-speed rotor topology design should be 335.58 MPa. Meanwhile, the yield strength of the high-strength NGO is 569.48 MPa and the maximum allowable stress for the high-speed rotor design can be 474.56 MPa considering the safety factor of 1.2. Consequently, under the same centrifugal force limit, the high-strength rotor can adopt a thinner magnetic bridge structure to reduce magnetic leakage and enhance the electromagnetic performance.

The test results of the ring sample are shown by the solid line in Fig. 6, and it can be seen that the stress–strain curves of the two groups of ring samples are basically consistent with the standard stress–strain curves. Through the adjustment of which, the design of the ring sample can basically satisfy the condition, where both sides of the sample are subjected to a uniform tensile stress. According to the comparison results in Fig. 6, the material elongation can be reduced by the topology of the ring sample. This phenomenon is caused by the ring sample topology. Comparing the sample after rupture, it can be observed that the testing material samples can produce plastic deformation on the surface of the material when tensile stress exceeds the yield strength.

From the comparison between the standard samples and the ring samples, we can discover that both sides of the ring sample, which wound with coil, are subjected to a large and relatively uniform tensile stress. Same plastic deformation zone appears on the surface of the ring samples [shown in Fig. 7(a)]. According to the stress–strain curves of the ring sample in Fig. 7(b), the obvious curve mutations are observed due to the bending deformation of the ring sample. Therefore, in the subsequent experiments, the topology of the ring sample can be further optimized.

It can be seen from the results of experiment 3 that there is a gap of 0.3–0.5 T in the saturation magnetic density of the B–H curves between the ring sample testing means and the standard Epstein means. This can be explained by the sensitivity decrease of the experimental equipment as well as the thickness reduction of the ring sample lamination. Both methods can make the NGO soft magnetic material reach the saturation. Therefore, the magnetic characteristics measured by the ring sample method, adjusted by the Epstein method, are merely in the B-axis. The B–H curves obtained with different ac frequencies in experiment 3 are shown in Fig. 8. It can be seen that the tensile stress can reduce the maximum flux density while the excitation frequency can raise the coercivity as predicted.

The results of experiment 4 are shown in Figs. 9 and 10, where two surfaces indicate the total iron loss of ten pcs laminated ring sample under various frequency and tensile stress when the magnetic field strength $H = 800$ A/m. The two surfaces have been fit by the surface smoothing functions, and the actual measurements are reflected by the solid points for each material. It can be seen that the iron loss of the NGO materials can be reduced by the tensile stress at different frequencies. For the conventional NGO material in the control group with the excitation frequency of 1000 Hz, the iron loss can reduce by 41.0% under the tensile stress of 235.71 MPa. With the excitation frequency of 100 Hz, the iron loss can

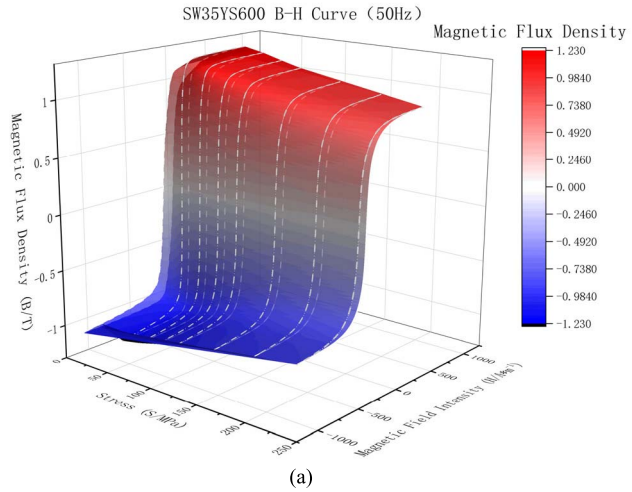

Fig. 8. B–H curves excited with ac source among various frequencies. (a) B–H curve with different tensile stress at 50 Hz. (b) B–H curve with different tensile stress at 100 Hz. (c) B–H curve with different tensile stress at 800 Hz.

reduce by 17.7% under the tensile stress of 235.71 MPa. For the high-strength NGO material in the experimental group with excitation frequency of 1000 Hz, the iron loss can reduce by 27.4% under the tensile stress of 235.71 MPa. When the

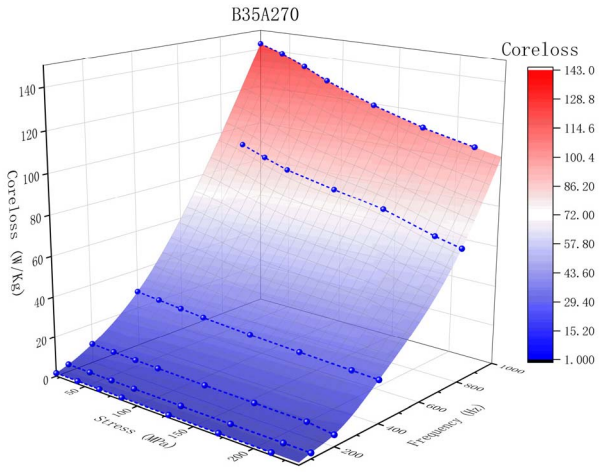

Fig. 9. Core loss characteristics of B35A270 under the combined influence of tensile stress and excitation frequency at $H = 800$ A/m.

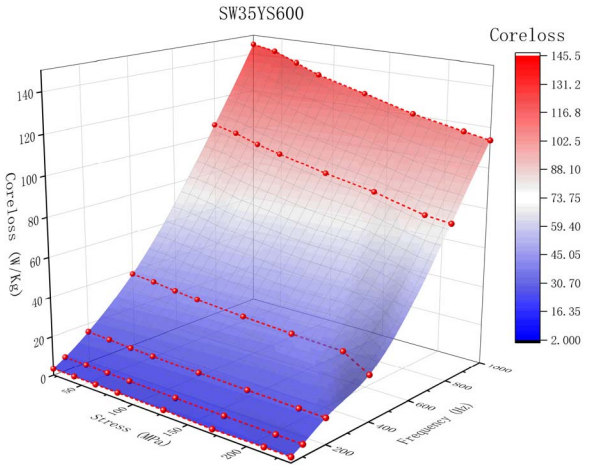

Fig. 10. Core loss characteristics of B35A270 under the combined influence of tensile stress and excitation frequency at $H = 800$ A/m.

excitation frequency is 100 Hz, the iron loss can reduce by 20.7% under the tensile stress of 235.71 MPa.

It can be observed that through the experimental results in experiment 4, the improvement of iron loss due to tensile stress for both NGO materials increases with the frequency. With the tensile stress, the improvement ratio of the iron loss of the two materials is rather different. This can be explained as the high yield strength ability of the high-strength NGO is partially attained by annealing process, and the annealing can cause the stronger residual internal stress, which can impede the formation of 180° magnetic domain with high permeability under the application of tensile stress.

IV. Conclusion

In this article, high-strength NGO material has been applied to high-speed IPMSM design. The application of new material should be conducted under customized design matched with the new material, instead of simple replacement with the conventional material under the same parameter design. The systematic optimization method presented in this article aims at making the best use of new material.

Through FEM simulation analysis, the benefit of high-strength NGO for rotor optimization in high-speed IPMSM is identified, together with the limitation of this optimization. It is revealed that the employment of high-strength NGO can cause iron loss concentration, and is subjected to tensile stress due to rotor PM centrifugal force. Experiment has been designed and conducted to measure the iron loss characteristics of NGO material with various frequency and tensile stress. Experiment results indicate that the iron loss of high-strength NGO has reduced by 27.4% under 1000 Hz frequency. The shortcoming of iron loss concentration can be significantly relieved due to centrifugal tensile stress, and rotor topology optimization with high-strength NGO application can be beneficial. The experimental samples are fabricated by wire-cutting technique, while in the actual process of lamination producing, the NGO sheet is fabricated by the punching process. The reduction of magnetic bridge dimension will raise residual shear stress. As a result, the edge effects will arise and the punching will affect a greater proportion of the lamination sheet.

Further works to be done are as follows.

1) Due to the limitation of experiment instrument, iron loss over 1000 Hz has not been tested, and, more experiment data can be achieved with better equipment.
2) According to the ring sample tensile experiment result, better topology can be proposed to avoid the bending deformation.
3) Different high-strength NGO can be tested, such as SW35YS900, B35AHS500, and 35HXT680T.
4) Characteristics of NGO under various temperatures can be meaningful, under the condition that the independent variables become temperature, stress, frequency, and magnetic field.
5) Pressure stress can be applied to the ring sample, which benefits the formation of 90° magnetic domain.
6) IPMSM prototypes, which adopt customized tensile stress concentrated rotor design, are being developed, so that the simulation result can be further validated.

ACKNOWLEDGMENT

This work was supported in part by Shanghai Outstanding Technology Leaders Plan under Grant 17XD1423400. The authors would like to thank their colleagues Yueshun Yuan, Lihui Wang, and Xiangjian Zhang for supporting the sample fabrication and testing. They would also like to thank Dongyang An from Shougang Steel Group, Beijing, China, who provides the high-strength silicon steel sample.

REFERENCES

[1] L. Situ, "Electric vehicle development: The past, present & future," in *Proc. 3rd Int. Conf. Power Electron. Syst. Appl. (PESA)*, May 2009, pp. 1–3.
[2] Y. Oda, M. Kohno, and A. Honda, "Recent development of non-oriented electrical steel sheet for automobile electrical devices," *J. Magn. Magn. Mater.*, vol. 320, no. 20, pp. 2430–2435, Oct. 2008.
[3] S. Cicale, L. Albini, F. Parasiliti, and M. Villani, "Design of a permanent magnet synchronous motor with grain oriented electrical steel for direct-drive elevators," in *Proc. 20th Int. Conf. Electr. Mach.*, Sep. 2012, pp. 1256–1263.
[4] P. B. Reddy, A. M. El-Refaie, S. Galioto, and J. P. Alexander, "Design of synchronous reluctance motor utilizing dual-phase material for traction applications," *IEEE Trans. Ind. Appl.*, vol. 53, no. 3, pp. 1948–1957, May 2017.
[5] M. Tietz, F. Herget, G. von Pfingsten, S. Steentjes, K. Telger, and K. Hameyer, "Effects and advantages of high-strength non grain oriented (NGO) electrical steel for traction drives," in *Proc. 3rd Int. Electric Drives Prod. Conf. (EDPC)*, Oct. 2013, pp. 1–6.
[6] I. Tanaka, H. Nitomi, K. Imanishi, K. Okamura, and H. Yashiki, "Application of high-strength nonoriented electrical steel to interior permanent magnet synchronous motor," *IEEE Trans. Magn.*, vol. 49, no. 6, pp. 2997–3001, Jun. 2013.
[7] J. Gong and H. W. Luo, "Progress on the research of high-strength non-oriented silicon steel sheets in traction motors of hybrid/electrical vehicles," *J. Mater. Eng.*, vol. 43, no. 6, pp. 102–112, Jun. 2015.
[8] T. Kubota, "Recent progress on non-oriented silicon steel," *Steel Res. Int.*, vol. 76, no. 6, pp. 464–470, Jun. 2005.